# Constraint-based semi-autonomy for unmanned ground vehicles using local sensing

Sterling J Anderson*[a], Sisir B. Karumanchi[a], Bryan Johnson[b], Victor Perlin[b], Mitchell Rohde[b], Karl Iagnemma[a]
[a]Massachusetts Institute of Technology, 77 Mass. Ave., Cambridge, MA USA 02139;
[b]Quantum Signal LLC. 200 N. Ann Arbor St., Saline, MI USA 48176

## ABSTRACT

Teleoperated vehicles are playing an increasingly important role in a variety of military functions. While advantageous in many respects over their manned counterparts, these vehicles also pose unique challenges when it comes to safely avoiding obstacles. Not only must operators cope with difficulties inherent to the manned driving task, but they must also perform many of the same functions with a restricted field of view, limited depth perception, potentially disorienting camera viewpoints, and significant time delays. In this work, a constraint-based method for enhancing operator performance by seamlessly coordinating human and controller commands is presented. This method uses onboard LIDAR sensing to identify environmental hazards, designs a collision-free path homotopy traversing that environment, and coordinates the control commands of a driver and an onboard controller to ensure that the vehicle trajectory remains within a safe homotopy. This system's performance is demonstrated via off-road teleoperation of a Kawasaki Mule in an open field among obstacles. In these tests, the system safely avoids collisions and maintains vehicle stability even in the presence of "routine" operator error, loss of operator attention, and complete loss of communications.

**Keywords:** Semi-Autonomy, Adaptive Autonomy, Teleoperation, Unmanned Ground Vehicles, Driver Assistance

## 1. INTRODUCTION

Teleoperated unmanned ground vehicles (UGVs) are playing an increasingly important role in the nation's next-generation ground forces. Their ability to grant access to areas that are unsafe for or inaccessible to humans has led to their integration in a variety of military functions, ranging from surveillance and reconnaissance to the detection and removal of hazardous materials.

While the advantages of teleoperation are compelling from tactical and human capital perspectives, the challenges associated with remotely operating a vehicle given current technology are daunting. Teleoperated vehicles are typically operated from a control station in which an operator monitors data transmitted from the vehicle and issues commands to it. Not only must the human operator cope with the challenges inherent to the manned driving task, but he/she must perform many of the same functions with a restricted field of view (FOV), limited depth perception, potentially disorienting camera viewpoints, and significant time delays. Telenavigating a ground vehicle under these conditions while monitoring the vehicle's health status, the status of the mission/tasks, and the condition of the environment leads to high failure rates. In a study of 10 field tests, UGV performance was shown to be relatively low, with mean time between failures ranging from 6 to 20 hours [1]. Given standard USAR and Department of Defense shifts of 12 and 20 hours, respectively, these results suggest that today's UGVs cannot be reliably depended upon to complete an entire shift [1].

Semi-autonomous control offers a unique opportunity to improve the human performance through the exploitation of human-automation synergies. As originally published in 1951 [2] and widely discussed since, humans and automation are uniquely well suited to specific types of tasks [3]. Whereas automation excels at responding quickly and precisely to well-defined or repetitive control objectives, humans tend to make more mistakes as the frequency and complexity of the control task increase. Conversely, humans have the unique ability to detect and contextualize patterns and new information, reason inductively, and adapt to new modes of operation, whereas automation typically struggles at these tasks. The goal of semi-autonomy is to exploit synergies in the abilities of humans and automation to improve planning and control performance of the combined system and – where possible – the actors therein.

Unmanned Systems Technology XIV, edited by Robert E. Karlsen, Douglas W. Gage,
Charles M. Shoemaker, Grant R. Gerhart, Proc. of SPIE Vol. 8387, 83870K
 · doi: 10.1117/12.919265

### 1.1 Previous work

Recent work on improving the reliability of teleoperated vehicles has focused largely on sensor processing and human interface design. Because of its substantial impact on wirelessly-teleoperated UGVs, much of this research has been devoted to reducing time delay and its perceived effects. Predictive displays using augmented reality, visual tracking, and image-based rendering or "virtualized reality" have been shown in many studies to improve UGV driving performance by 20-60% over standard (live video feed) teleoperation control [4–6]. Further performance improvements have been achieved using multimodal displays [7] and multimodal inputs [8].

While advances in sensor processing and human interface design may improve the operator's distance estimation, spatial orientation, and object detection, and may even reduce the effects of sensing and control latency, reliable UGV operation remains fundamentally limited by the perception, judgment, and driving skill of the human operator. Just as maturation in manned ground vehicle design has resulted in driver error becoming the sole factor in 60% of automobile accidents and a contributing factor in 95% [9] so it is expected that maturation in UGV instrumentation and interface design will ultimately result in driver error being the limiting factor in the performance of teleoperated vehicles [10]. Further improvements in the safety and reliability of both manned and unmanned ground vehicles will come from control systems with enough autonomy to correct, override, or reduce the occurrence of driver error.

Incorporating autonomy into a teleoperated vehicle presents two unique challenges for which traditional autonomous planning and control techniques are ill-suited. First, common autonomous vehicle control architectures operate as layered subsystems, first planning and then tracking a collision-free path without accounting for or providing an effective means of cooperating with a human operator [11–15]. This reliance on specific paths is fundamentally at odds with the field-based planning and control technique humans have long been shown to exhibit [16]. Rather than obsessively planning and tracking a single path, humans tend instead to identify a field of safe travel – one that contains an infinite number of continuously deformable ("homotopic") paths – and control the vehicle within it. On an open roadway, for example the preferred homotopy often contains many acceptable paths traversing a desired lane. In off-road environments, the chosen homotopy may not be so clear, though vehicle dynamic constraints require that it exclude any region through which the vehicle cannot travel without colliding with obstacle(s). Arbitrarily confining the vehicle to a specific path when many safe paths exist can be over restrictive for a human operator. Figure 1 illustrates three prominent homotopies in a cluttered environment as perceived by a human operator.

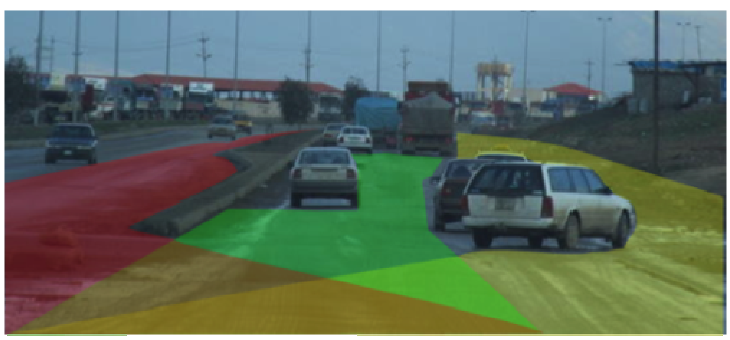

Figure 1. Visualization of prominent homotopies available to a human operator (image best viewed in color).

The second challenge facing shared control is that adding some degree of autonomy to the vehicle can disorient a human operator or throw off his mental model of the vehicle's response characteristic. In this work, a haptic feedback method was designed to reduce this mismatch by applying suggestive torques to the operator's steering wheel interface.

## 2. SEMI-AUTONOMY BASED ON HOMOTOPIC CLASSES

The semi-autonomous controller presented in this work is designed to allow the teleoperator significant control freedom within an available homotopic class, intervening only as necessary to avoid collisions with obstacles. This control requires the identification of safe and dynamically feasible homotopic classes, the calculation of threat (or the need for control intervention to prevent collisions), and the coordination of operator and controller commands to ensure that obstacles are avoided without unduly restricting the control freedom of the human operator.

### 2.1 Vision-based identification of homotopic classes

In this work, a vehicle-mounted Velodyne LIDAR is used to identify collision hazards in the vehicle's environment. These hazards are circumscribed by bounding boxes, and the remaining free space is partitioned into a complete set of adjacent rectangular cells. An optimal "channel" (a sequence of dynamically-reachable cells with the greatest total area) spanning from the vehicle's current location to the distal edge of the sensing window is then calculated using dynamic programming. Figure 2 illustrates these cells and the constraints designed to bound homotopy $\mathrm{H} = \mathbf{A}_1 \cup \mathbf{A}_2 \cup \mathbf{A}_3 \cup \mathbf{A}_4 \cup \mathbf{A}_7 \cup \mathbf{A}_6 \cup \mathbf{A}_9$.

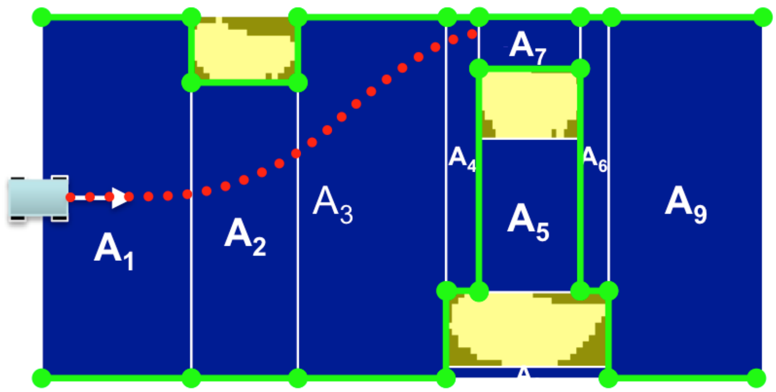


Figure 2: Illustration of environment map, homotopy selection, and constraint delineation. Yellow regions indicate obstacles, green lines indicate upper and lower bounds on the lateral position of the vehicle, and the red dotted trajectory represents the MPC prediction.

### 2.2 Threat assessment from homotopy constraints

In the previous section, an objective function was defined to assess the goodness of a given homotopy. Once a desired homotopy has been identified, vehicle position constraints circumscribing the homotopy must be converted into semi-autonomously enforceable constraints on the human operator's control inputs as the vehicle traverses the constrained region.

To calculate these limits, a finite-horizon model predictive (MPC) controller incorporating the aforementioned position constraints is used to predict the vehicle state evolution under a stability-optimal control input sequence. The nearness of this predicted trajectory to stability limits is then used to compute the steering constraint applied at the vehicle and the torque feedback returned to the operator.

The controller used in this work bases its predictions on a 4-wheeled vehicle model with slip and yaw dynamics. Defining vehicle states, outputs, inputs, and disturbances by **x**, **y**, **u**, and **v**, respectively, discrete plant dynamics are described by

$$\mathbf{x}_{k+1} = \mathbf{A}\mathbf{x}_k + \mathbf{B}_u\mathbf{u}_k + \mathbf{B}_v\mathbf{v}_k \tag{1}$$

$$\mathbf{y}_k = \mathbf{C}\mathbf{x}_k + \mathbf{D}_v\mathbf{v}_k \,. \tag{2}$$

A quadratic objective function over a prediction horizon of p sampling intervals is defined as

$$J_k = \sum_{i=k+1}^{k+p} \frac{1}{2}\mathbf{y}_i{}^{\mathrm{T}}\mathbf{R}_y\mathbf{y}_i + \sum_{i=k}^{k+p-1} \frac{1}{2}\mathbf{u}_i{}^{\mathrm{T}}\mathbf{R}_u\mathbf{u}_i + \sum_{i=k}^{k+p-1} \frac{1}{2}\Delta\mathbf{u}_i{}^{\mathrm{T}}\mathbf{R}_{\Delta u}\Delta\mathbf{u}_i + \frac{1}{2}\rho_\varepsilon\varepsilon^2 \tag{3}$$

where $\mathbf{R_y}$, $\mathbf{R_u}$, and $\mathbf{R}_{\Delta\mathbf{u}}$ represent diagonal weighting matrices penalizing deviations from $\mathbf{y}_\mathrm{i} = \mathbf{u}_\mathrm{i} = \Delta\mathbf{u}_\mathrm{i} = 0$, $\rho_\varepsilon$ represents the penalty on constraint violations, $n$ denotes the number of free control moves, and ε represents the maximum constraint violation over the prediction horizon $p$. Inequality constraints on vehicle position (**y**), inputs (**u**), and input rates (**Δu**) are then defined as:

$$
\begin{gathered}
\mathbf{y}^{j}{}_{\min}(i)-\varepsilon\mathbf{V}^{j}{}_{\min}(i)\leq\mathbf{y}^{j}(k+i+1\,|\,k)\leq\mathbf{y}^{j}{}_{\max}(i)+\varepsilon\mathbf{V}^{j}{}_{\max}(i)\\
\mathbf{u}^{j}{}_{\min}(i)\leq\mathbf{u}^{j}(k+i+1\,|\,k)\leq\mathbf{u}^{j}{}_{\max}(i)\\
\Delta\mathbf{u}^{j}{}_{\min}(i)\leq\Delta\mathbf{u}^{j}(k+i+1\,|\,k)\leq\Delta\mathbf{u}^{j}{}_{\max}(i)\\
i=0,\dots,p-1\\
\varepsilon\geq 0
\end{gathered}
\tag{4}
$$

where the vector $\Delta\mathbf{u}$ represents the change in input from one sampling instant to the next, the superscript "$(\bullet)^j$" represents the $j^{\text{th}}$ component of a vector, $k$ represents the current time, and the notation $(\bullet)^j(k+i|k)$ denotes the value predicted for time $k+i$ based on the information available at time $k$. The vector $\mathbf{V}$ allows for variable constraint softening over the prediction horizon, $p$, when ε is included in the objective function. The vectors $\mathbf{y}^{\mathbf{y}}_{\min}$ and $\mathbf{y}^{\mathbf{y}}_{\max}$ are sampled from the edges of the constrained channel $\mathbf{H}^n$. Also note that input constraints enforced in the MPC calculation are simply those imposed by available actuation.

The state trajectory $\bar{x}$ predicted by the MPC solution represents the state evolution of maximum stability that can be achieved given the vehicle's current position, dynamics, and homotopy constraints (imposed by $\mathbf{H}^n$). As such, the nearness of this prediction's stability-critical states to their physical limits provides a useful indication of the need for intervention and a natural boundary for the current vehicle input. Here, we define by "threat", Φ, the maximum predicted value of a stability-critical state (front wheel sideslip in this case). We then adjust the steering command seen by the vehicle to

$$u_{vehicle}=K(\Phi)u_{MPC}+(1-K(\Phi))u_{driver}, \tag{5}$$

where $K\in[0\quad 1]$ is computed using a piecewise linear function which ensures that at low threat, the vehicle closely matches operator commands, and at high threat (when the safest maneuver satisfying homotopy constraints approaches the limit of vehicle stability), the vehicle steering command tracks the optimal command predicted by the MPC controller. For a complete treatment of the threat assessment and the shared control method used in (5), the reader is referred to the authors' previous work in [17].

In addition to the constraint imposed on (or adjustment made to) the vehicle steering (which is transparent to the human operator), experimental tests also fed back a tactile set of "soft" constraints on the position of the steering wheel. This feedback provides a greater situational awareness to the human operator, particularly in teleoperation scenarios, as it indicates not only where the input constraints lie, but also how urgently they must be satisfied in order to avoid collision or loss of control. The resistance torque applied to the operator's steering wheel is calculated as

$$\mathrm{T}=k_{\max}K\left|\delta_{driver}-\delta_{MPC}\right| \tag{6}$$

where $k_{max}$ represents the maximum available steering wheel torque and is used to re-dimensionalize $K$. Figure 3 illustrates the response of the torque restoring function to increasingly threatening MPC predictions.

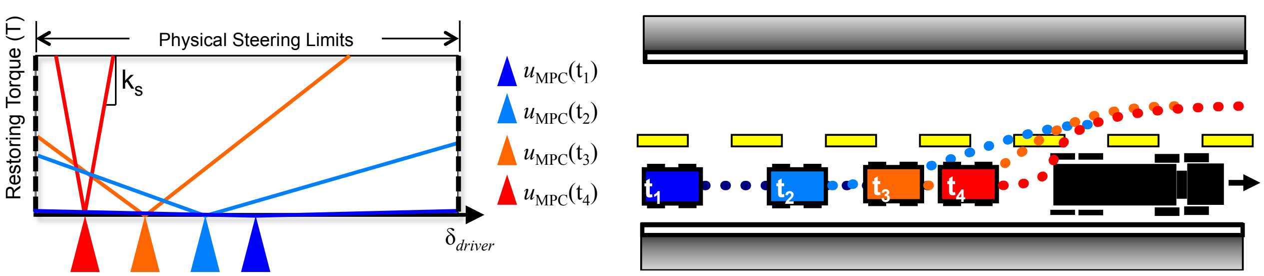


Figure 3. Scenario illustration showing the response of the restoring torque function as a vehicle successively approaches a hazard from behind

Notice that as time progresses (denoted by $t_i$ labels on the host vehicle), the threat posed by the optimal maneuver prediction increases in severity. Additionally, the immediate steering command required to track this optimal trajectory begins to drift leftward. The combined effect of an increasingly-urgent, and progressively-leftward $u_{MPC}$ recommendation increases $k_s$ and shifts the torque resistance trough. In the limiting case for which only the optimal steering command can reasonably be expected to avoid both the hazard and loss of control (sometime shortly after $t_4$), the controller exerts the maximum available torque on the operator's steering wheel, essentially ensuring that the operator not only cedes to the requirements of the controller, but is also aware of exactly what steering action is being taken by the vehicle.

Figure 4 shows block diagrams for the semi-autonomous control system with and without torque feedback. The basic configuration is referred to as *Scaled intervention* (Figure 4a). Figure 4b shows a configuration of the system with torque feedback to the user. Figure 4c shows a hybrid system that combines scaled intervention with torque feedback.

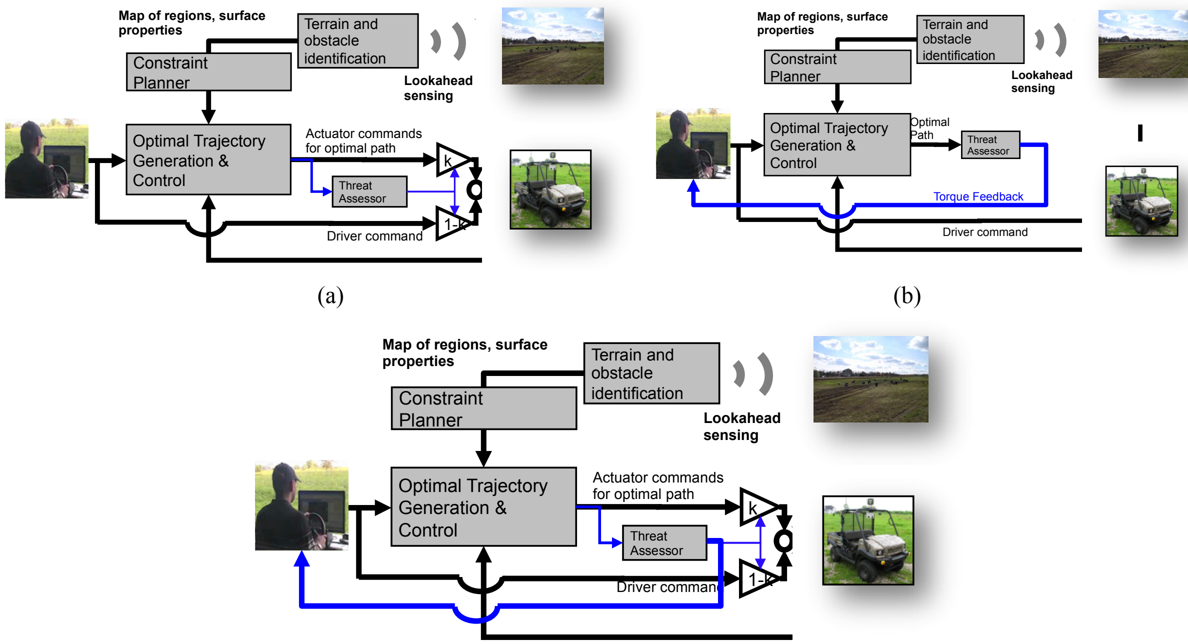


(a) (b) (c)

Figure 4: a) Block diagram for direct "Scaled Intervention" (SI) system b) torque-based feedback system, and c) combined system

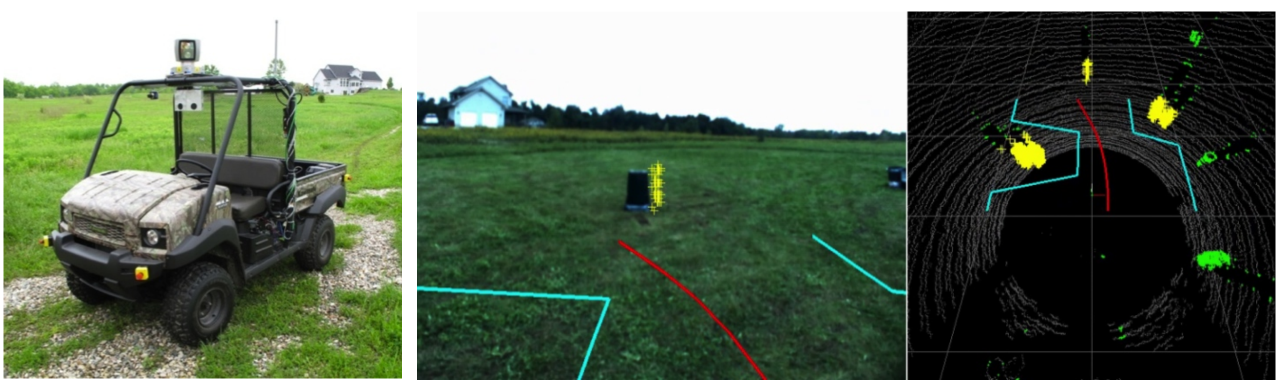

(a) (b)

Figure 5: (a) Kawasaki 4010 Mule Test Platform; (b) Local constraint planner and MPC implementation: Planned local constraints (cyan) and predicted path (red) displayed in camera and LIDAR views, respectively.

## 3. EXPERIMENTAL RESULTS

Experimental testing was performed on a Kawasaki 4010 Mule (see Figure 5a) fitted with steering and braking actuators, an omnidirectional video head, Velodyne LIDAR, NavCom GPS, and a triaxial IMU. An onboard Linux PC ran controller code and transmitted video and other data to a teleoperator control station over an 802.11g wireless link. At the remote control station, a teleoperator received video and state feedback data on a computer monitor and issued steering commands through a Logitech G27 steering wheel. Torque constraints were applied to the steering wheel via its dual-motor force feedback mechanism capable of applying 0-3.1 N-m of torque in either direction. Barrels were arranged on an open field as obstacles and the teleoperator was instructed to navigate the vehicle without hitting them.

Results under two experimental scenarios are discussed below. First, the scaled intervention (SI) system (Figure 4(a)) is assessed under artifically induced time delays to assess performance in long-range remote tele-operation. Second, high-speed obstacle avoidance performance of the different control configurations shown in Figure 4 is compared.

In the first set of experiments, a fixed artificial time delay was introduced and the operator was instructed to navigate the vehicle between selected waypoints at increasing time delays while avoiding obstacles. Figure 6(a)-(b) shows the trajectories under different artificially induced time delays with (b) and without (a) operator assistance.

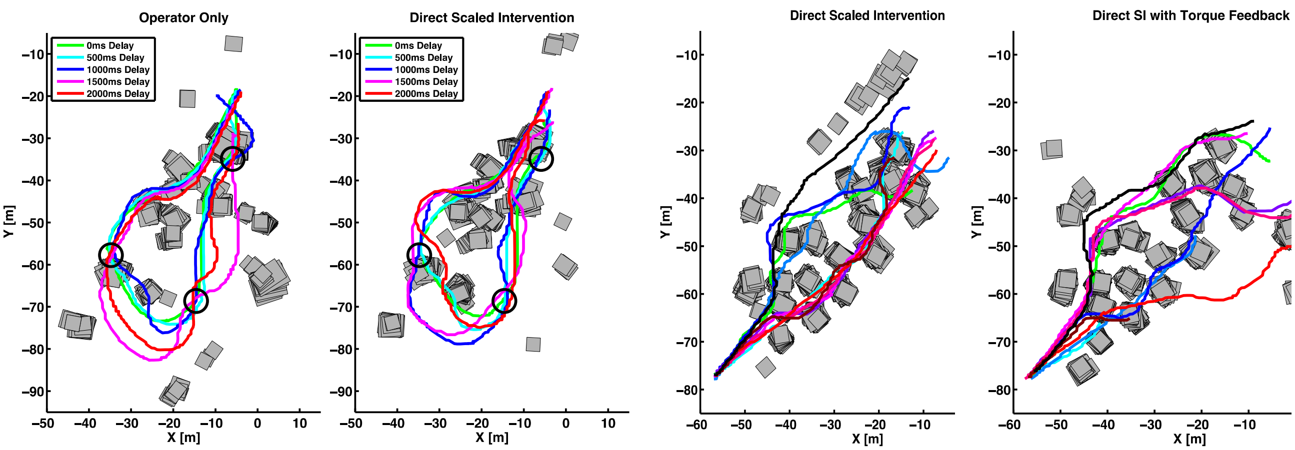


(a) (b) (c) (d)

Figure 6: (a)(b) Results of assisted and unassisted waypoint navigation tests conducted with varying time delays. Waypoints are shown as black circles. (c)(d) Comparison of high speed obstacle avoidance under different operator assistance configurations. Note that the obstacles shown in the figures are transformations of locally sensed obstacles into the global frame. The obstacle locations are only approximate due to a mediocre navigation solution with a low cost IMU.

Figure 7 compares key performance metrics across assisted and unassisted runs. Notice that for all communication delays, the assisted system outperformed its unassisted control group. The top left plot shows average velocity of the runs which is improved under assisted operation. With assistance, the operator was able to drive faster given an increased confidence in his ability to avoid collisions. The remaining plots (RMS vehicle steer angle - bottom left; Max vehicle steer angle – top right; avg. steer angle commanded by the driver – bottom right), demonstrate a reduction in the intensity of steering corrections from the driver to avoid obstacles. The user's control inputs were more moderate, leading to more consistent routes and fewer run-ins with hard steering constraints (±30°).

The second set of experiments required the operator to traverse a dense obstacle field at speeds close to 18 km/hr without hitting obstacles. In this test, neither waypoints nor a specific route were specified; the operator's mission was to reach a goal line at the distal edge of the field. Figure 6(c)-(d) shows the trajectories of navigation tests with (d) and without (c) torque feedback in the obstacle field.

Table 1 summarizes the success rate of navigation tests conducted with varying control strategies and in the presence of various communication-related challenges. Navigation without any assistance resulted in a 5% success rate. Under direct SI, a success rate of 70% was achieved. Torque feedback alone only demonstrated a success rate of 40%. In isolation, the torque feedback mechanism is not able to address loss of communication and time delays. However, a combined system of SI and torque feedback (shown in Figure 4b) demonstrated a success rate of 70% which is on par with the SI system. In addition, the combined system provides the operator with improved situational awareness, resulting in his report of an improved understanding of the control actions being taken/suggested by the controller.

The failures observed under semi-autonomous control were due to sensing limitations; in regions with high obstacle density, the 3m x 3m blind spot of the Velodyne sensor lost track of obstacles, resulting in constraints that did not preclude their position. Upgrading the inertial navigation hardware should allow the sensing algorithm to maintain obstacle locations in a global frame and thereby avoid failures like these.

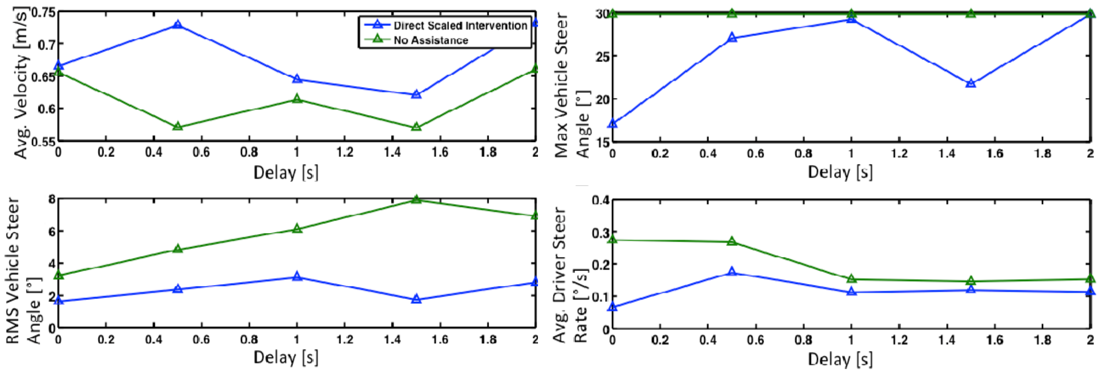


Figure 7: Comparison of assisted and unassisted performance as a function of communication time delay

Table 1: Minefield results summary

| **Success Rate (%)*** | No Assistance | Direct SI | Torque Assistance | Direct SI + Torque |
|---|---|---|---|---|
| Loss of Vision | 5% | 70% | 40% | 70% |
| Loss of Comms | 5% | 70% | – | 70% |
| Delay | 0%** | 63%** | – | – |

* Sample size = 10 ** Sample size = 8

## 4. CONCLUSION

Semi-autonomous navigation requires planning and control methods capable of identifying desirable path homotopies and ensuring that the controlled system remains within them. This paper has illustrated a methodology for achieving minimally-restrictive, homotopy-based control through the planning and enforcement of constraints – rather than reference paths – on the states and control inputs of the vehicle. Experimental results were presented that assessed multiple semi-autonomous control architectures on an unmanned Kawasaki Mule operating in an outdoor environment under various communication-related challenges. A torque feedback mechanism in isolation was shown to be insufficient as it did not compensate for loss of communication and cannot handle time delays. In contrast, the scaled intervention architecture was shown to effectively assist a human driver in avoiding collisions even under severe time delays. A combined architecture was proposed that coupled scaled intervention with torque feedback. This architecture provides the same guarantees as the SI methodology while providing improved situational awareness to the user. Finally, while the results shown here are promising, further work studying the feasibility and "goodness" of path homotopies and the effects of various input constraint enforcement techniques on the performance and situational awareness of human drivers remain to be conducted.

## ACKNOWLEDGMENTS

The authors would like to thank James Walker, Dan Rice, Kevin Melotti, and Rob Lupa for their assistance in setting up the Mule test vehicle and conducting experiments. This material is based upon work supported by the U.S. Army Research Laboratory and the U.S. Army Research Office under contract/grant number W911NF-11-1-0046, as well as DARPA DSO under the M3 program.

## REFERENCES


[1] J. Carlson and R. R. Murphy, "How UGVs physically fail in the field," *Robotics, IEEE Transactions on*, vol. 21, no. 3, pp. 423–437, 2005.

[2] P. M. Fitts, M. S. Viteles, N. L. Barr, D. R. Brimhall, G. Finch, E. Gardner, W. F. Grether, W. E. Kellum, and S. S. Stevens, "Human engineering for an effective air-navigation and traffic-control system, and appendixes 1 thru 3," Mar. 1951.

[3] T. B. Sheridan and R. Parasuraman, "Human-Automation Interaction," *Reviews of Human Factors and Ergonomics*, vol. 1, no. 1, pp. 89 –129, Jun. 2005.

[4] A. Kelly, N. Chan, H. Herman, D. Huber, R. Meyers, P. Rander, R. Warner, J. Ziglar, and E. Capstick, "Real-time photorealistic virtualized reality interface for remote mobile robot control," *The International Journal of Robotics Research*, vol. 30, no. 3, pp. 384–404, 2010.

[5] D. Kim, S. Kim, J. Kim, C. Lee, and J.-O. Park, "Active operator guidance using virtual environment in teleoperation," in *Proc. of the 1998 IEEE/RSJ International Conference on Intelligent Robots and Systems*, Victoria, Canada, 1998, vol. 2, pp. 1084–1089.

[6] Zhenyuan Deng and M. Jagersand, "Predictive display system for tele-manipulation using image-based modeling and rendering," in *Proceedings of the 2003 IEEE/RSJ International Conference on Intelligent Robots and Systems*, Piscataway, NJ, USA, 2003, vol. vol.3, p. 2797–802.

[7] J. Aleotti, S. Caselli, and M. Reggiani, "Multimodal user interface for remote object exploration with sparse sensory data," in *Proc. of 11th IEEE International Workshop on Robot and Human Interactive Communication*, 2002, pp. 41– 46.

[8] D. Weimer and S. K. Ganapathy, "A synthetic visual environment with hand gesturing and voice input," in *Conference on Human Factors in Computing Systems*, USA, 1989, p. 235–40.

[9] L. Evans, "The dominant role of driver behavior in traffic safety.," *Am J Public Health*, vol. 86, no. 6, pp. 784–786, Jun. 1996.

[10] S. Domme, P. Hwang, P. Kim, M. Wang, and B. Sperling, "A value based approach to determining top hazards in army ground vehicle operations," in *2006 IEEE Systems and Information Engineering Design Symposium*, Charlottesville, VA, United states, 2007, pp. 124–129.

[11] J. Leonard, J. How, S. Teller, M. Berger, S. Campbell, G. Fiore, L. Fletcher, E. Frazzoli, A. Huang, S. Karaman, O. Koch, Y. Kuwata, D. Moore, E. Olson, S. Peters, J. Teo, R. Truax, M. Walter, D. Barrett, A. Epstein, K. Maheloni, K. Moyer, T. Jones, R. Buckley, M. Antone, R. Galejs, S. Krishnamurthy, and J. Williams, "A perception-driven autonomous urban vehicle," *Journal of Field Robotics*, vol. 25, no. 10, pp. 727–774, 2008.

[12] R. Vaidyanathan, C. Hocaoglu, T. S. Prince, and R. D. Quinn, "Evolutionary path planning for autonomous air vehicles using multiresolution path representation," in *Proc. of IROS 2001*, Maui, HI, United States, 2001, vol. 1, pp. 69–76.

[13] Dong Kwon Cho and Myung Jin Chung, "Intelligent motion control strategy for a mobile robot in the presence of moving obstacles," in *Proc. IROS '91*, New York, NY, USA, 1991, p. 541–6.

[14] L. B. Cremean, T. B. Foote, J. H. Gillula, G. H. Hines, D. Kogan, K. L. Kriechbaum, J. C. Lamb, J. Leibs, L. Lindzey, C. E. Rasmussen, A. D. Stewart, J. W. Burdick, and R. M. Murray, "Alice: An information-rich autonomous vehicle for high-speed desert navigation," *Journal of Field Robotics*, vol. 23, no. 9, pp. 777–810, 2006.

[15] A. Bemporad, M. Morari, V. Dua, and E. N. Pistikopoulos, "The explicit linear quadratic regulator for constrained systems," *Automatica*, vol. 38, no. 1, pp. 3–20, 2002.

[16] J. J. Gibson and L. E. Crooks, "A Theoretical Field-Analysis of Automobile-Driving," *The American Journal of Psychology*, vol. 51, no. 3, pp. 453–471, Jul. 1938.

[17] S. J. Anderson, S. C. Peters, T. E. Pilutti, and K. Iagnemma, "An Optimal-Control-Based Framework for Trajectory Planning, Threat Assessment, and Semi-Autonomous Control of Passenger Vehicles in Hazard Avoidance Scenarios," *IJVAS*, vol. 8, no. 2–4, pp. 190–216, 2010.